Multi-Input Isolated Power Converter for Electric Vehicles with Hybrid Energy Storage

Kandaswamy K V[1,*], Shyam D[2], Sivamani D[2]
[1]*Department of Electrical and Electronics Engineering, Murugappa Polytechnic College,*
[2]*Department of Electrical and Electronics Engineering, Rajalakshmi Engineering College, Thandalam, Chennai, Tamil Nadu, India*
[*]*kvksamys@gmail.com; shyam.d@rajalakshmi.edu.in; sivamani.d@rajalakshmi.edu.in*

***Abstract*—The existing converter relies on a non-isolated transformer and lacks bidirectional support in the case of multiple and regenerative inputs. The proposed work focuses on an isolated multiport bidirectional DC-DC converter topology featuring a battery and a supercapacitor for an electric vehicle (EV) of 2 kW. The proposed topology can provide uninterrupted power to the EV's electric motor and recover braking energy, allowing bidirectional power flow. As a result, the battery discharge time can increase due to the additional source, such as a supercapacitor and regenerative action. The system integrates two single H-bridge converters at the input and a single H-bridge converter at the output, with an existing switch. The converter enables the reduction of the rated voltages of the battery and supercapacitor packs. Additionally, a power-flow management scheme and its corresponding control scheme are proposed. The performance test has been conducted on traditional and PI control methods under different operating conditions with a switching frequency of 50 kHz, such as switching power from the battery or supercapacitor to the load during driving and from the load back to the source during energy generation. Power flow capabilities and efficiency values validate the viability and effectiveness of the proposed system of 2 kW.**

***Index Terms*—Bidirectional converter; Electric vehicle; Isolating transformer; Regenerative braking; Supercapacitor.**

I. INTRODUCTION

The full-bridge bidirectional converter (FBBC) is a flexible power-electronic topology commonly used in applications requiring bidirectional power flow. This converter is essential in systems such as renewable energy integration, electric vehicles (EVs), energy storage systems (ESS), and microgrids [1]. The FBBC facilitates efficient energy transfer between two DC sources or between a DC source and an AC grid, making it a critical component in modern power systems. The FBBC consists of four switching devices (typically MOSFETs or IGBTs) arranged in a full-bridge configuration. These switches are controlled to regulate the direction and magnitude of power flow.

The converter operates in two primary modes: it transfers energy between storage units, such as batteries and supercapacitors, while also providing electrical isolation and protection for the system. This makes it an essential part of modern renewable energy systems, electric vehicles, and other high-power applications, where the ability to manage multiple energy sources and sinks is critical to optimal performance [2]. This function is particularly important in applications where energy storage systems must respond quickly to changes in load or source power, thus ensuring a stable and efficient energy supply. The isolated full-bridge bidirectional converter (IFBBC) is crucial for this purpose because it enables efficient energy transfer between the battery and the supercapacitor [3], maintaining stable output voltage and current under varying conditions. It can supply a load of approximately 2 kW when the main power source is unavailable, capture excess energy from the load, and store it efficiently [4], thus maximizing overall system efficiency. Additionally, IFBBC provides electrical isolation between input and output, as shown in Fig. 1, which is important for safety and reliability in high-power applications [5].

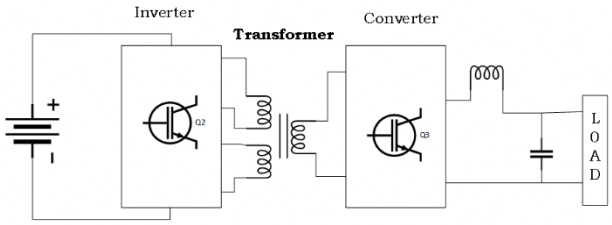


Fig. 1. General block diagram.

Nkwanyana, Siti, Wang, Toudjeu, Mbungu, and Mulumba [6] reviewed hybrid energy storage systems for renewable energy applications, emphasizing battery-supercapacitor integration to improve efficiency, reliability, and battery life. The study highlighted the need for advanced energy management strategies to address sizing, control, and cost optimization challenges. Hua and Lai [7] suggested that the bidirectional power transfer and reduced battery current ripple. The converter achieved up to 94 % efficiency with soft-switching operation, making it suitable for battery energy storage and DC microgrid applications. Xu, Liu, Yan, and Yang [8] proposed an adaptive terminal sliding mode control strategy for a fuel cell-battery-supercapacitor hybrid energy storage system to achieve robust power sharing under parameter uncertainties.

Huang *et al.* [9] proposed that the IFBBC topology offers high efficiency, galvanic isolation, and bidirectional power transfer capability. It consists of a full-bridge inverter, a high-

Manuscript received 2 February, 2026; accepted 30 March, 2026.

frequency transformer, and a full-bridge rectifier, which allows DC-DC conversion with high efficiency. While many studies highlight the synergy between batteries and supercapacitors in HESS, there is disagreement about the optimal pairing. The research by Hao *et al.* raises concerns about the degradation mechanisms in lithium-ion batteries resulting from rapid charge-discharge cycles driven by the high-frequency operations of the supercapacitor. Strategies for dynamic switching among storage elements remain under investigation [10]. Yu, Liu, Min, Sun, and Xu [11] use fuzzy logic control to ensure adaptive power distribution between the battery and SC without requiring an accurate mathematical model. Farajdadian, Hajizadeh, and Soltani [12] proposed that multi-input isolated DC-DC converters (MICs/multi-port DC-DC) have gained attention for electric vehicles (EVs) because they allow integration of on-board charging, traction power conversion, and auxiliary power in a single transformer-isolated stage, reducing the number of parts and improving the density of packaging compared to multiple independent converters. Recent surveys indicate that three-port architectures, namely, dual active bridge (DAB) derivatives and triple/three-winding active bridges (TAB), are dominant choices for bidirectional, high-power automotive applications. DAB-based three-port designs (including series/resonant variants and interleaved implementations) provide flexible bidirectional power flow via phase-shift or multi-variable modulation; TAB and other three-winding topologies reduce switches/rectifiers at the cost of more complex magnetics and coupling control. The choice of topology trades off isolation, achievable ZVS range, magnetics complexity, and part count; recent comparative studies show that one- and three-phase DAB variants perform differently when scaled to 100 kW class systems, Guennouni, Machkour, and Chebak [13], which point to the need to evaluate loss sources and transformer design early in architecture selection. Wangsupphaphol, Phichaisawat, Nik Idris, Jusoh, Muhamad, and Lengkayan [14] propose control approaches ranging from classical phase-shift and duty-cycle modulation to model-based decoupling, sliding-mode, and model-predictive control for multi-port power sharing.

Energy management systems (EMS) that determine power splits between the battery and SC are often developed independently of the converter inner-loop controllers: EMS operate on a slower supervisory timescale, whereas the converter executes rapid power tracking and enforces device constraints. Reviews of HESS controllers document numerous EMS heuristics (rule-based, fuzzy, and optimization), but co-designed EMS-converter control with formal guarantees remains comparatively rare. Work on fault-tolerant multi-port converters focuses on detection and reconfiguration strategies. Still, papers rarely map fault handling and control reconfiguration directly to ISO 26262 automotive safety goals (ASIL decomposition, FMEA/FMEDA). Practical automotive qualification requirements (redundant sensing, safe shutdown sequencing, and port isolation under fault conditions) are only partially addressed in the academic literature by Negri, Ubezio, and Faranda [15].

The goal of this research paper is to investigate the design and operation of a specialized converter that integrates batteries and supercapacitors in a combined energy storage system. By examining the technical nuances and potential applications of this converter, we aim to demonstrate how it can enhance energy efficiency, reliability, and longevity in various applications.

II. PROPOSED METHOD OF ISOLATED FULL BRIDGE CONVERTER (IFBC)

An isolated full-bridge bidirectional converter (IFBC) is a power electronic converter that enables the transfer of electrical energy between two circuits while providing electrical isolation. This type of converter is commonly used in applications such as battery storage, electric vehicles, and renewable energy systems [16]. The IFBC consists of two inverters and a converter, and vice versa; the inverter section consists of four switches (typically MOSFETs or IGBTs) arranged in a full-bridge configuration [17]. These switches control the direction of current flow [18]. On the converter or output side, a rectifier (usually a diode bridge) converts the AC output from the transformer back to DC. The next section comprises an isolation transformer that provides electrical isolation between the input and output of the converter [19]. It also helps in voltage step-up or step-down, depending on the ratio of turns. The control circuit manages the switching of the full-bridge inverter and regulates the output voltage and current. Finally, inductors and capacitors may be used to filter the output voltage and current, reducing ripple and improving quality.

Compared to a non-isolated multiport DAB/TAB converter, the proposed IFBC topology offers better system integration and allows for hybrid and bidirectional operation. This work shows stable power operation, regenerative action, and coordination between the battery and supercapacitor. It also reduces battery stress and lowers source-voltage needs, while simplifying magnetic and control requirements compared to traditional multiport DAB/TAB converters.

A. Operating Principle of the Proposed IFBC

The operation of the isolated full-bridge bidirectional converter shown in Fig. 2 can be divided into two main modes: forward and reverse mode [20], [21]. In forward mode, i.e., Buck Mode (V1 > V2), two diagonal switches of the full-bridge inverter are turned on alternately. For example, switches S1 and S4 can be turned on while S2 and S3 are off, and then S2 and S3 can be turned on while S1 and S4 are off. This action induces an alternating current in the primary winding of the transformer. Alternating current in the primary winding induces a voltage in the secondary winding of the transformer, which is then rectified to a DC output by the diode bridge. Energy flows from the input side (e.g., a battery or solar panel) to the output side (e.g., a load or another battery) in this mode.

During Interval 1 (t0 - t1) on the inverter side, the switches Q1 and Q2 are turned ON. Q3 and Q4 are OFF. This applies a positive voltage (+V1) to the battery through the primary winding of the transformer. Similarly, switches Q1’ and Q2’ are turned ON. Q3’ and Q4’ are OFF. This procedure applies a positive voltage (+V2) across the primary winding of the transformer for the supercapacitor in Fig. 3. This, in turn, applies two voltages ON on the primary side.

On the rectifier side, switches Q5 and Q6 are ON, while

switches Q7 and Q8 are OFF. The transformer secondary voltage (V2' = V1 * N2/N1) is applied to the output capacitor C2, charging it and supplying current to the load connected to V2. The equivalent circuit in this mode consists of a voltage V1/N across the capacitor C2.

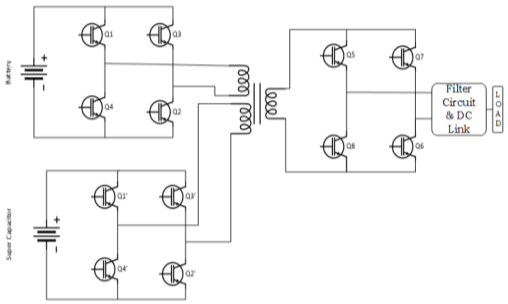


Fig. 2. Multi-input integrated isolated DC-DC converter.

Dead Time/Transition Period will occur at interval 2 (t1 - t2), and during this stage, Q1 and Q2 are turned OFF, and Q3 and Q4 are turned OFF for the interval (t3 - t4). All switches are OFF on the inverter side. All switches are OFF. The current in the leakage inductance Ll continues to flow, thereby charging and discharging the unwanted switch capacitances, potentially enabling zero-voltage switching. On the rectifier side, Q1 and Q2 are turned ON, Q3 and Q4 are OFF, and then Q3 and Q4 are turned ON. Q1 and Q2 are OFF for the interval (t3 - t4). The leakage inductance provides current continuity to the load.

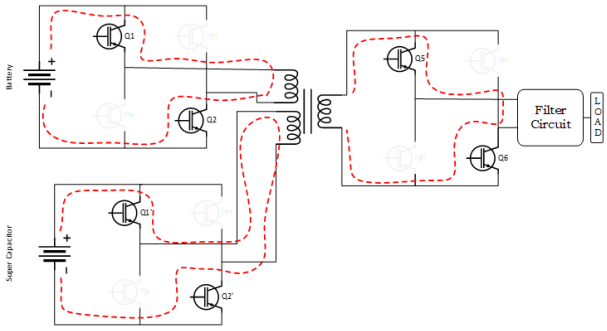


Fig. 3. Battery and supercapacitor supply the voltage to the load. Positive switches are triggered "ON".

Similarly, during Interval 3 (t2 - t3), switches Q3 and Q4 are turned ON on the inverter side, as shown in Fig. 4. Q1 and Q2 are OFF. This applies a negative voltage (-V1) to the primary winding of the transformer.

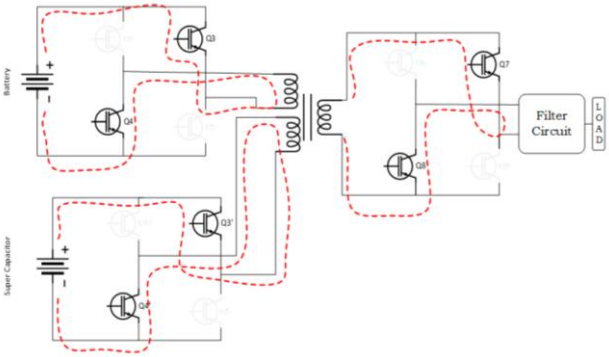


Fig. 4. Battery and supercapacitor supply the voltage to the load, and the negative switches are triggered "ON".

In reverse mode, i.e., Boost Mode (V2 > V1), the operation is similar, but the control circuit changes the switching sequence to allow the current to flow in the opposite direction. For example, Q7 and Q8 can be turned ON while Q5 and Q6 are OFF, as shown in Fig. 5. At the same time, the high-voltage side, which is the rectifier side, has switches Q5 and Q6 turned ON. Q7 and Q8 are OFF, as shown in Fig. 6. The transformer secondary voltage (-V2' = -V1 * N2/N1) is applied to the output capacitor C2, charging it and supplying current to the load. In this mode, the equivalent circuit consists of a source voltage of the -V1/N charging capacitor C2.

The current now flows in the opposite direction through the transformer, inducing a voltage in the secondary winding that is also rectified to produce a DC output. In this mode, energy flows from the output back to the input, which is useful for applications such as regenerative braking in electric vehicles or battery charging from a load.

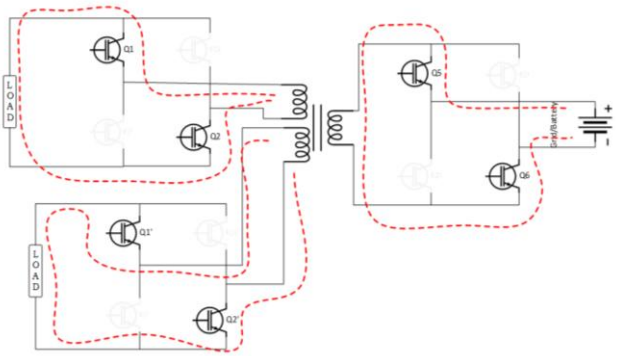


Fig. 5. Load supplies the voltage to the source during the regenerative action (battery and supercapacitor), during which positive switches are triggered "ON".

At the same time, the high-voltage side (i.e., rectifier side) switches Q5 and Q6 are turned ON. Q7 and Q8 are OFF, as shown in Fig. 6. The transformer primary voltage (V1' = V2 * N1/N2) is applied to the output capacitor C1, charging it and supplying current to the load connected to V1.

During Interval 3 (t2 - t3), the low-voltage side switches Q3 and Q4 on the inverter side are turned ON, while Q1 and Q2 remain OFF. This procedure applies a negative voltage (- V2) on the secondary winding of the transformer. Similarly, switches Q3' and Q4' are turned ON. Q1' and Q2' are OFF. This applies a negative voltage (-V2) to the secondary winding of the transformer.

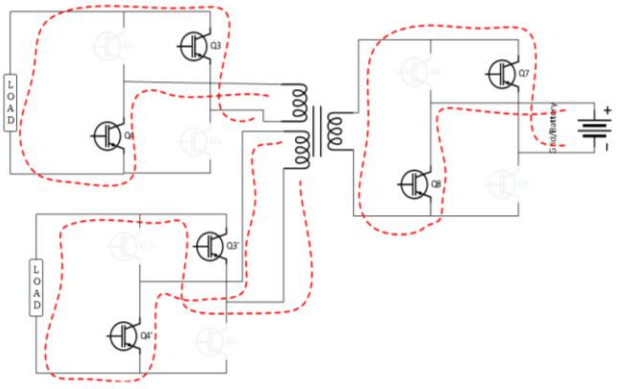


Fig. 6. Load supplies the voltage to the source during the regenerative action (battery and supercapacitor) while negative switches are triggered "ON".

At the same time, the high-voltage side, which is the rectifier side, has switches Q7 and Q8 turned ON while Q5 and Q6 remain OFF. The primary voltage of the transformer (-V1' = -V2 * N1/N2) is applied to the output capacitor C1, charging it and supplying current to the load. The Dead Time/Transition Period occurs at Intervals 4 (t3 - t4) and 2 (t1-t2); it is similar to Buck Mode.

The proposed method achieves better functional integration by using a simpler design, which has fewer switches and less cascading. Also, using a single transformer reduces magnetic complexity and reduces overall system cost compared to a traditional system. Improved coordination between the battery and supercapacitor helps increase energy use. As a result, the overall efficiency of the system will improve. The proposed system includes a supercapacitor, which reduces thermal stress and loading effects on the battery, thus improving the reliability of the system.

B. Mathematical Equation for Analysis and Design of the Proposed System

For a dual active bridge (DAB) between two ports (say, battery and DC bus), the power transferred is [22]

$$P = \frac{nV_1V_2}{\omega L}\cdot\sin(\phi), \tag{1}$$

where V1, V2 are the voltages on the primary and secondary sides, n is the turn ratio, ω is the angular frequency of the transformer voltage waveform, L is the leakage inductance, and ϕ is the phase shift between the primary and secondary voltages.

This is the same form as the grid power-angle equation: $P = \frac{V_1V_2}{X}\cdot\sin(\delta)$. In isolated converters (e.g., DAB with sinusoidal link current), L is the leakage/series inductance, nV2 is the reflected secondary voltage, and phase shift φ is the control knob for P.

This equation holds for all port-to-port transfers:

– Battery to DC bus;
– Supercapacitor to DC bus;
– Battery to Supercapacitor (if supported).

The total load power P_{load} is met by both sources as follows

$$P_{load} = P_{bt} + P_{sc}, \tag{2}$$

where P_{bt} is the battery power contribution and P_{sc} is the supercapacitor power contribution.

Using a sharing ratio $\alpha \in [0, 1]$:

$$P_{bat} = \alpha \times P_{load}, \tag{3}$$

$$P_{sc} = (1-\alpha)\times P_{load}. \tag{4}$$

This can be adjusted dynamically on the basis of State of Charge (SoC), current demand, or efficiency targets.

For the proposed converter operating at approximately 2 kW output power, Pout = 2000 W.

The switching loss per switch is approximated by Psw = 0.5 × Vds × Id × (tr + tf) × fs, assuming:

– Vds = 140 V;
– Id = 15 A;
– tr + tf = 120 ns;
– fs = 50 kHz;
– Psw ≈ 50.4 W for 8 switches;
– Pcond ≈ 70 W with approximately switching resistance 0.08;
– Ptrans ≈ 30 W with approximately cu and core loss;
– Passive loss ≈ 5 W considering very little leakage inductance;
– Total Ploss ≈ Psw + Pcond + Ptrans;
– Total Ploss ≈ 50.4 + 70 + 30+5 =155.4 Watts.

Total Efficiency ≈ 92.7 % approximately after taking the loss in the account.

The proposed topology is expected to reach a peak efficiency of about 93 % to 95 % during optimized and phase-shift operation. The percentage of loses is shown in Fig. 7. This represents an improvement of 2 % to 4 % compared to conventional systems. Additionally, combining a battery with a supercapacitor increases power density by around 15 % to 25 %. This boost comes from reducing the number of magnetic components, filters, and converter stages.

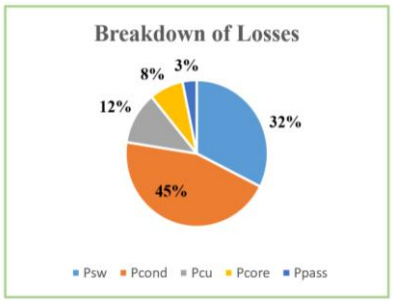


Fig. 7. Various breakdown losses.

C. Battery and Supercapacitor Dynamics

Assuming ideal conditions and focusing on energy exchange:

Battery dynamics (energy source):

$$dE/dt = -P_{bt}, \tag{5}$$

$$E_{bt} = C_{bat}\cdot(V_{bt})/2; \tag{6}$$

Supercapacitor dynamics (fast-response energy buffer):

$$dvsc/dt = i_{sc}/C_{sc}, \tag{7}$$

$$P_{sc} = v_{sc}\times i_{sc}, \tag{8}$$

where C_{sc} is the capacitance of the supercapacitor, i_{sc} is the current into the supercapacitor, v_{sc} is the voltage of the supercapacitor, and E_{bat} is the energy stored in the battery.

D. Control-Oriented Model (State-Space)

The fundamental inductor equation is as follows

$$V_L = Ldi/dt, \tag{9}$$

where V_L is the instantaneous voltage across the inductor (in volts), L is the inductance (in henries, H), and di/dt is the rate of change of the inductor current (A/s).

From this, we can rearrange as follows

$$di/dt = V_L/L. \tag{10}$$

The inductor (L) net voltage is the difference between the two voltages

$$V_L = V_{bt} - n_{bd} V_{dc}. \quad (11)$$

where V_{bt} is the battery voltage or primary side reflected voltage from a transformer, n_{bd} is the turns ratio factor from a transformer or coupled inductor, and V_{dc} is the DC bus voltage or secondary side voltage.

The term $n_{bd}V_{dc}$ represents the reflected voltage on the inductor side due to the transformer coupling. This difference (V_{bt} - $n_{bd}V_{dc}$) is the net voltage pushing current through the inductor.

Now, substituting $V_L = V_{bt} - n_{bd}V_{dc}$ into the general form,

$$di_L / dt = V_{bt} - n_{bd} V_{dc} / L_{bd}. \quad (12)$$

E. Multi-Loop Control Scheme of the Proposed Method

The controller of the proposed system is designed to handle several control tasks, such as managing power flow, controlling the battery, controlling the supercapacitor, and controlling the DC link, as shown in Fig. 8.

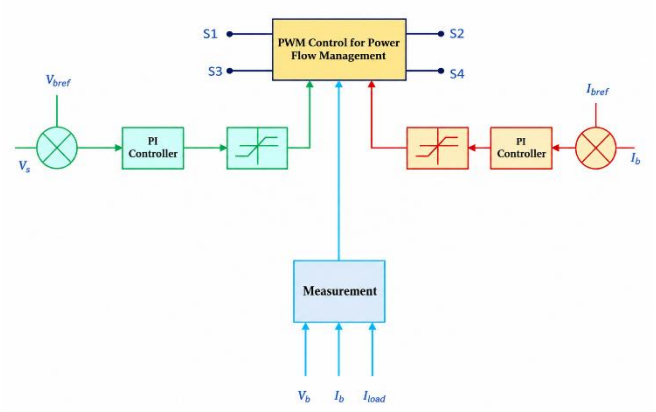


Fig. 8. Control structure of the proposed method.

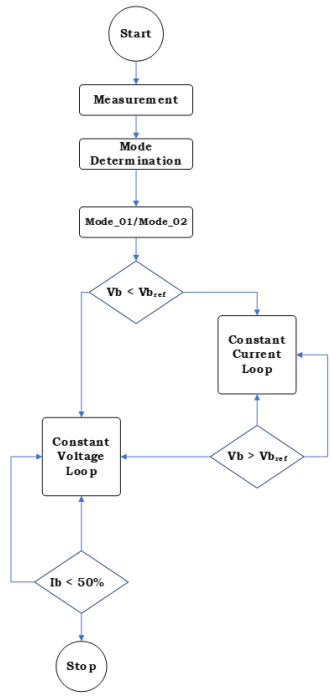


Fig. 9. proposed block diagram of multi-input integrated isolated DC-DC converter.

The ability of the controller to send power from the ESU, SC, and battery to the EM makes it possible for the best power flow to occur between these three parts [23]. The main goals of power flow management are the following:

1. To ensure that the EM continues to provide power while taking into account the SC and battery limits;
2. To ensure that the braking energy is recovered by providing reverse power flow [24].

The power flow management method allocates system operating modes based on available battery and SC power, EM demand, ESU status, and EM-requested power (PEm). The flow chart of the control strategy is shown in Fig. 9.

F. Pseudocode for the Control Strategy

The power management approach determines the operating modes of the system considering the available power from the battery and SC [25], the EM demand, and the ESU state, including the required power of the EM (PEm).

Algorithm 1. Dual feedback PI control with PWM-based power flow management.

```
begin
  // Step 1: Measurement inputs
  measure (Vb, Ib, I_Load)
  // Step 2: Voltage control loop
  error_V ← V_ref - Vb
  control_signal_V ← PI_Controller (error_V)

  modulated_signal_V ← Modulator (control_signal_V)
  // Step 3: Current control loop
  error_I ← I_ref - Ib
  control_signal_I ← PI_Controller (error_I)
  modulated_signal_I ← Modulator (control_signal_I)
  // Step 4: Power flow management using PWM
  pwm_control (
     input_from_voltage_loop = modulated_signal_V,

     input_from_current_loop = modulated_signal_I,
     measurement_feedback = {Vb, Ib, I_Load}
  )
  // Step 5: Generate switching signals
  generate_switches (S1, S2, S3, S4)
end
```

III. METHOD OF OPERATION

Mode 1: The combined power from the battery (PBt) and supercapacitor (Psu) power is the maximum power requirement of the EM (PEm), as shown in Fig. 9. In this case, the excess energy present in the battery storage (PBt) is delivered to the load, i.e., to EM through the ESU. The equations show that the load voltage is determined by both the battery and the supercapacitor, which supply the EM system via the energy storage unit (ESU).

The switches Q3 and Q4 operate at a constant duty cycle of 50 %, resulting in a 180 ° phase difference between them. The duty cycles of the complementary switches Q1 and Q2 vary with the parameters set by the power flow control system. The temporal disparity between Q1 and Q2/Q3 facilitates DC-link regulation, while the varying duty cycles of Q1 and Q2 optimize power delivery by modulating the output voltage or enabling bidirectional energy flow for the energy storage unit. The controller monitors the output voltage and current of the integrated source and computes the available instantaneous power. The various switchings of the

input condition is shown in Fig. 10.

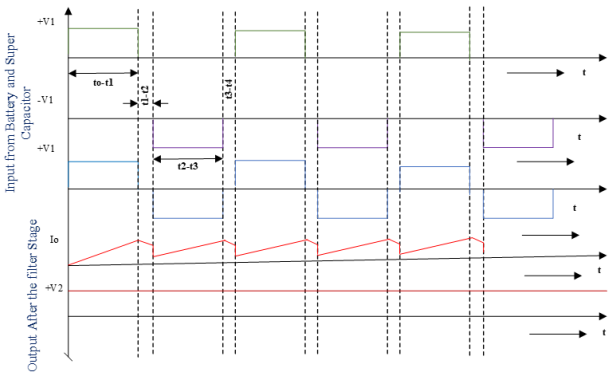


Fig. 10. Switching sequence: when both sources are acting.

The various stages of the proposed method are explained in detail (Fig. 11). It comprises four stages, from the inverter to the converter.

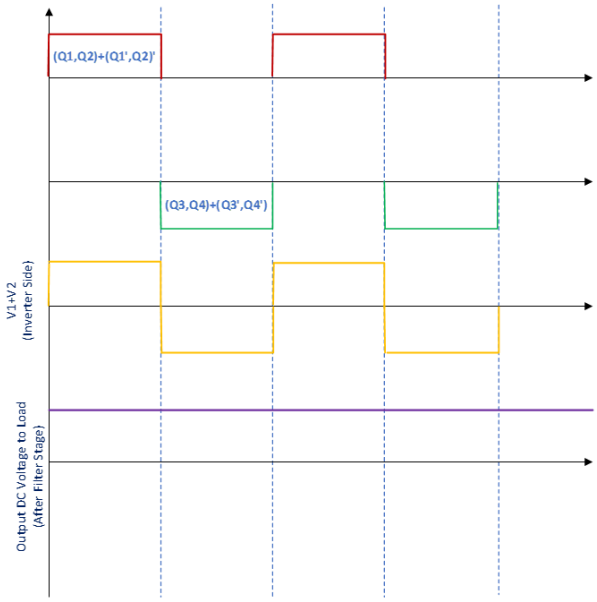


Fig. 11. Various stages of the switching sequence.

Stage 1: In stage 1, both the battery and the supercapacitor supply voltage to the load [26]. During this stage, the converter operates as an inverter from the source to the isolating transformer; the positive switches are turned ON, and the load side is converted from AC to DC. The output voltage is constant since the LC filter is used on the load side. The current ripples are due to the load conditions.

Stage 2: During this stage, both the battery and the supercapacitor supply the voltage continuously, but the switching transition occurs between the positive and negative switches. The load voltage remains stable because the current continuously circulates through the load. The current decays for a short period before it goes to zero, negative switches are triggered, and the load receives a continuous voltage and current. This will make the load current continuous. The switching cycle will be selected to minimize the ripple current.

Stage 3: During previous stage 2, both the battery and the supercapacitor supply the load with voltage. During this stage, the converter operates as an inverter from the source to the isolating transformer; the negative switches are turned ON, and the load side output is converted from AC to DC. The output voltage is constant because an LC filter is used on the load side; current ripple arises from the load conditions.

Stage 4 is similar to the operation performed in stage 2. Then the cycle continues.

The substantial energy from the combined source (battery and supercapacitor) is delivered to the ESU through the CC-CV charging algorithms in Mode 1. The controller regulates the charging current to prevent it from exceeding 50 % of the battery pack capacity. Once the battery pack reaches the reference charge current (Ibref), the controller maintains a constant charge current [27]. Continuous current regulation will continue until the battery voltage reaches the reference value (Vbref). The procedure begins with charging at a constant current, and then proceeds to charging at a constant voltage. After this period, the charge current gradually decreases to 0.05 C, indicating that the charging cycle has ended. It is through the management of the duty cycles of switches Q1 and Q2 that the CC-CV charging process is completed. Furthermore, the CC-CV charging process is achieved by varying the duty cycles of the Q5 and Q6 switches when the circuit operates in Mode 3.

For each control, the difference between the measured current (Ib)/voltage (Vb) and the set reference current (Ibref)/voltage (Vbref) is found and used in the proportional-integral (PI) controllers for the constant current (CC) and constant voltage (CV) charging methods. As Mode 2 progresses, the ESU and the battery power the EM by controlling the DC-link reference voltage through their control loops. The DC-link driver changes the phase shift between Q2 and Q3 and between Q1 and Q4. The error is computed by subtracting the reference value of the EM DC-link voltage (Vdcref) from the recorded DC-link voltage (Vdc). The error signal is used by the PI controller to make the phase shift angle (ϕ).

IV. Results and Discussion

This section presents an evaluation of the performance of the proposed system. Isolated-gate bipolar transistors are switching elements in power circuits due to their power rating and switching frequency [28]. There are two reasons for this. The system presented is evaluated using two case studies. This method is used to conduct case studies to validate that the proposed system can operate in all modes. Mode 1 and Mode 2 are both represented by the first case, which also includes dynamic responses during the transition between the two modes.

The gating signals for the opposite pairs of switches at each port are controlled in a complementary manner. The simulation result for Mode 3 operation is shown, in which both the battery and supercapacitor are charged by the DC motor load, which operates as a DC generator in regenerative mode, as illustrated in Fig. 12. The state of charge of both the battery and supercapacitor increases. In regenerative mode, power is negative; therefore, torque is negative. From these results, bidirectionality and regenerative operation are inferred. The gating signal for the opposite pair of switches at each port is controlled in a complementary manner [29].

The different numerical values of the components used in MATLAB/Simulink for implementing the proposal are listed in Table I.

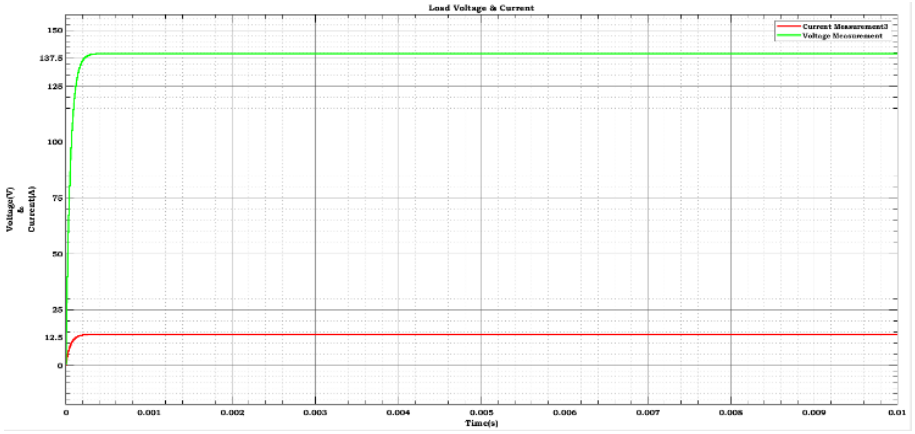


Fig. 12. The output voltage and current of the multiport bidirectional converter.

TABLE I. SYSTEM PARAMETERS FOR THE PROPOSED SYSTEM.

Component and Parameter Name	Value
Battery voltage (Vbt)	70 V
Supercapacitor voltage (Vsc)	70 V
DC bus/output voltage (Vdc)	140 V
Transformer turns ratio (n = N2/N1)	1:2
Leakage inductance (L)	120 µH
Output filter capacitance (Cdc)	2200 µF
Supercapacitor capacitance (Csc)	58 F
Battery equivalent capacitance model (Cbat)	40 Ah
Load resistance	Approximately 10 Ω at rated power

The simulation circuit diagram of a multiport isolated bidirectional DC-DC converter shown in Fig. 12 has three active ports: a battery on port 1 with a 70 V input, a supercapacitor on port 2 with a 70 V input and a 140 V output, and a 140 V output on port 3. All three ports are active bridges, and the switches are implemented using IGBTs. The simulation shows Mode 1 functioning, in which both the battery and the supercapacitor supply the resistive load. The simulation result for Mode 2 operation is illustrated above, with the battery in discharge mode, powering the load and the supercapacitor. The battery state of charge is decreasing, as shown in Fig. 13, while the supercapacitor is charging, as shown in Fig. 14. The supercapacitor starts at a charge of 93 % and has increased since then. Figure 14 shows that the supercapacitor port receives power, causing port 2 to have an output power equal to the negative of its actual value.

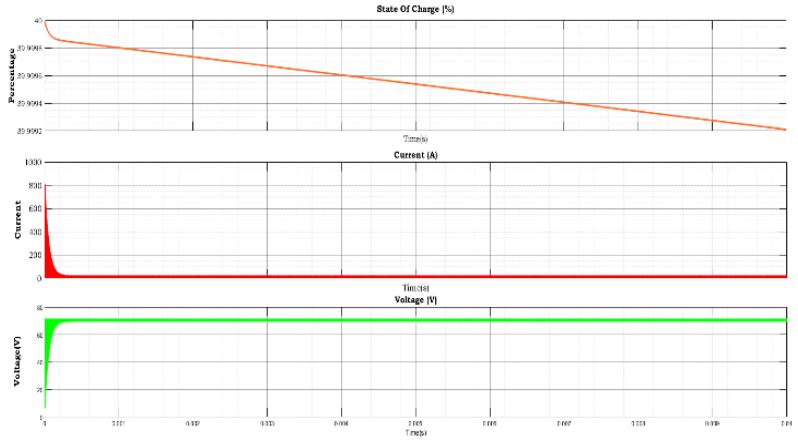


Fig. 13. Output response of the battery.

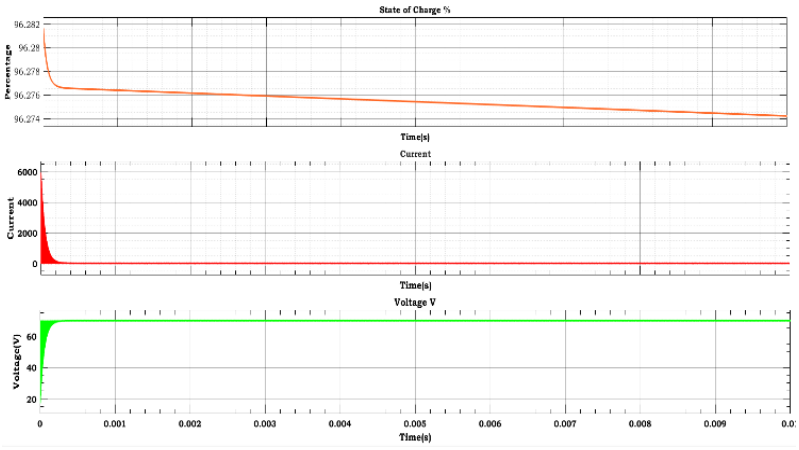


Fig. 14. Output response of the supercapacitor.

The proposed EV application used to boost along with a battery and a supercapacitor to control a voltage of 140 V. A transformer with a turn ratio of 1:2 was used. The leakage inductance of about 120 µH was selected to reduce the ripple current, allow soft switching, and limit the circulating current.

The supercapacitor value was chosen to support the rapid transient between the acceleration and the regenerative braking event and also to reduce the peak current stress on the battery.

The results above present the voltages and currents obtained under the different conditions. Figures 14 and 15 show the output voltage levels with and without PID, along with the response of the multiport converter. It is essential to study the various stress conditions that arise during converter operation. Table II briefly describes the voltages, currents, and thermal stresses obtained with a multiport converter.

In the closed-loop control technique, the gating signals are controlled with the help of a proportional plus integral (PI) controller, as shown in Fig. 16. This issue may arise from the limitations of the phase shift control technique, which are addressed by the pulse width modulation plus phase shift control technique, proposed as future work. The PID control technique also reduces the output voltage settling time and reduces the output ripple. Figure 17 shows the settling time and error for the PID and non-PID control methods.

The proposed control method combines two power sources into a single output voltage, using an isolation transformer to ensure that load requirements are met and to maintain stable operation. Change the topology (e.g., by using larger magnetic components and higher-voltage components), implement careful current sharing and interleaving, or replicate optimized power modules (typically 10 kW to 50 kW) to scale the system. For safety, serviceability, and manufacturing, modular replication is preferred. Figure 18 displays the efficiency of the proposed system under various operating conditions.

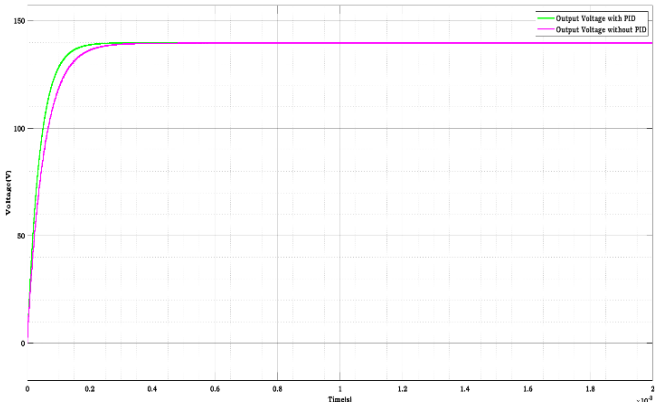


Fig. 15. Output response with and without a PID controller.

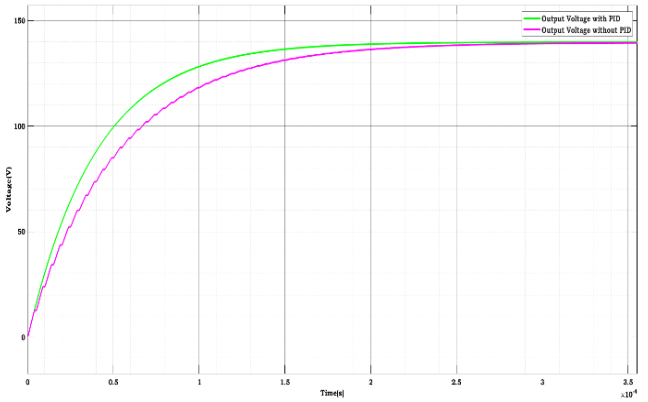


Fig. 16. Error between PID and without PID.

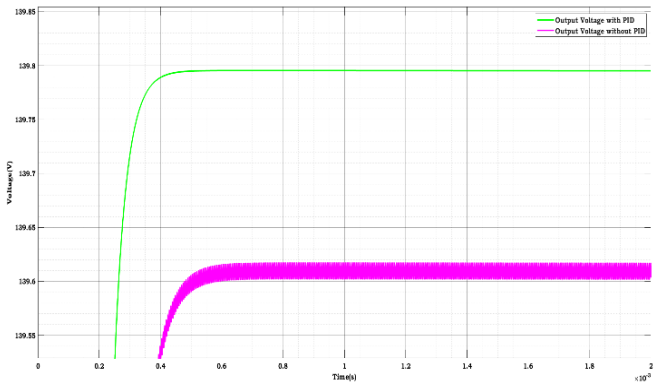


Fig. 17. Output voltage, settling time of the multiport bidirectional converter.

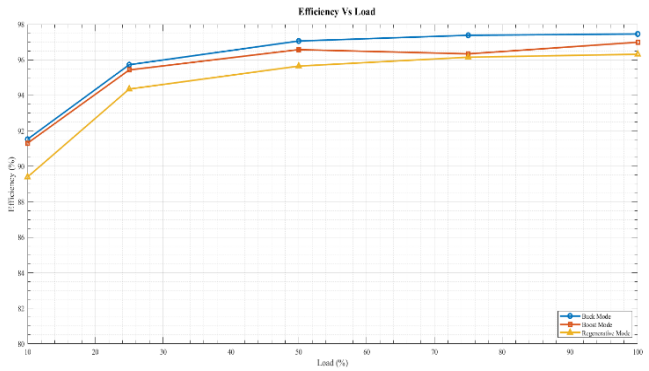


Fig. 18. Efficiency curve for different operating conditions.

TABLE II. VOLTAGE AND CURRENT STRESS OF THE PROPOSED TECHNIQUE.

Component	Voltage Stress	Current Stress	Key Conditions / Worst Case
Primary switches (battery/SC bridges)	≈ Port DC voltage VB, VSC (×1.6–2.0 margin). Overshoot ΔV from leakage + Coss	RMS ≈ IHF, RMS/ $\sqrt{2}$	V1-V2'
Secondary switches (active rectifier)	≈ Vo (×1.6–2.0 margin)	RMS ≈ Io/ $\sqrt{2}$, where Io = Ptot/Vo.	High output power, low bus voltage
Secondary diodes (if used)	Reverse ≈ 2×Vo	Avg ≈ Io/2, peak ≈ Ipk/n	Output surge/regeneration
HF Transformer (core)	Primary winding voltage = port DC	RMS = reflected HF current; peak = Ipk/n	High port voltage → core flux density; low port voltage → high RMS copper loss
Leakage Inductor (if external)	Clamped by port voltage	Carries full HF link current	Low port voltage & high power = worst RMS
Snubber/clamp	Limits overshoot: TVS ≈ 1.2–1.3×port V	Absorbs energy Eℓ=½LℓItr2	Worst at high current transitions
Thermal stresses	–	–	Concurrent battery + SC → circulating RMS rise

V. EXPERIMENTAL IMPLEMENTATION AND PERFORMANCE EVALUATION OF A PROPOSED METHOD

The proposed method was analyzed using MATLAB simulations with a battery and a supercapacitor. The schematic above was tested with a prototype model comprising a battery and a supercapacitor pack.

The hybrid energy storage system (HESS) test arrangement is shown in Fig. 19, which operates through a power electronic interface that connects a battery and supercapacitor system to a microcontroller. The system aims to combine battery energy storage with supercapacitor power delivery through its high-speed power delivery system to improve efficiency, power quality, and energy storage performance.

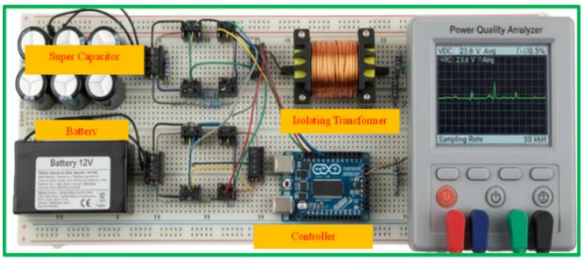


Fig. 19. Experimental implementation of the proposed method.

The proposed arrangement utilizes a 12 V battery as the primary energy source, tasked with meeting average and steady-state power requirements. The electrochemical properties of the battery make it vulnerable to deterioration due to frequent high-current transients. A controlled converter interface connects a supercapacitor bank to the system in parallel. The supercapacitor reduces the current load on the battery by providing or absorbing high peak currents, thus extending the battery lifespan through current relief.

The power electronic stage consists of high-frequency switching devices that operate under pulse-width modulation (PWM) signals generated by the controller. An isolating transformer is placed between the source and load sides to ensure galvanic isolation, enhance electrical safety, and facilitate voltage level matching. The system benefits from isolation, which decreases common-mode noise and enhances reliability for electric vehicle chargers, renewable energy systems, and grid-connected converter applications. The controller continuously monitors system parameters, including voltage, current, and State of Charge (SoC), while applying energy management to control the distribution of power from the battery and supercapacitor.

As a proof-of-concept platform, a 12 V experimental prototype was developed in Fig. 19. Its goal was to verify regenerative braking, bidirectional power flow, hybrid battery-supercapacitor coordination, and converter operation. The objective was not to precisely match the voltage level of a commercial EV. Rather, it sought to validate the working concept in an economical and secure laboratory environment.

The voltage stress on the primary switches increases approximately in proportion to the DC-link voltage when this design is scaled to contemporary EV platforms (400 V to 800 V). The voltage on the battery side, plus switching transients, is almost equal to the voltage stress on the prototype's primary switch. Moving to automotive voltage levels increases the voltage stress on the primary switch, but overall efficiency, improved power density, and reduced thermal loading are made possible by the decrease in current. If appropriate semiconductor ratings, insulation design, thermal management, and soft-switching control strategies are applied, the suggested IFBC architecture can scale to 400 V–800 V EV platforms.

Figure 20 shows the change in the battery and supercapacitor SoC during different loading conditions. The supercapacitor's SoC exhibits rapid fluctuations, demonstrating its ability to deliver brief power surges, while the battery's SoC declines steadily, supplying typical power needs. The hybrid system uses supercapacitors to handle sudden energy demands, preventing high-current loads from damaging batteries and enabling efficient power and energy management.

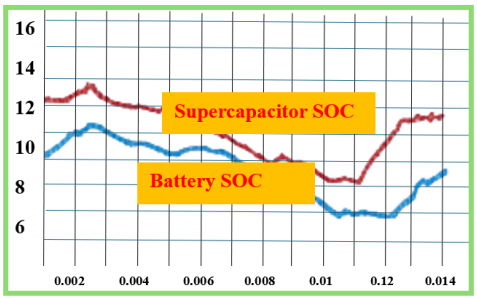


Fig. 20. SoC of the battery and supercapacitor.

The converter switching behavior produces different outputs, as shown in Fig. 21. The upper waveform shows the controller creating PWM gate signals at high frequency, while the lower waveform shows the converter current ripple or output. The supercapacitor implementation reduces voltage and current variations, which creates a more consistent waveform output. A power quality analyzer confirms the enhancement by showing stable voltage levels and reduced harmonic distortion.

The experimental results show that the hybrid energy storage system successfully improves the transient response, reduces battery deterioration, and enhances power quality. The system achieves high-performance energy storage by integrating batteries and supercapacitors, which operate through intelligent control systems and dedicated power conversion systems for electric vehicles, microgrids, and renewable energy systems.

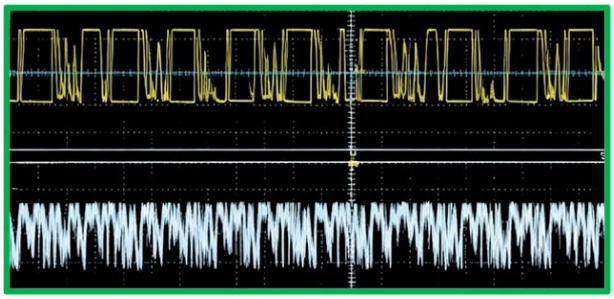


Fig. 21. PWM for inverter and converter, and vice versa.

VI. CONCLUSIONS

The isolated full-bridge bidirectional DC-DC converter is a versatile and efficient solution for applications requiring bidirectional power flow and electrical isolation. Understanding their step-by-step operation, switching

sequences, and control techniques is crucial for the design and implementation of these converters. This paper provided an in-depth primer on its operating principle, highlighting the key components and their roles in bidirectional power transfer. The results obtained at various levels indicate that the proposed control method ensures stable and effective operation of the EV during regenerative braking, thus supplying the load voltage to both the battery and the supercapacitor. Therefore, the converter manages both power transfer and power generation direction to ensure effective input and output. It helps reduce the discharge rate of both batteries during critical conditions. The battery life cycle will improve.

Since the proposed PI control technique is simple and efficient compared to nonlinear control methods, it is also easy to implement for practical EV applications. The system can rapidly achieve stability under various transient conditions, owing to the natural characteristics of the battery and supercapacitor energy storage elements. The duty cycles of the switches change according to sudden voltage changes on the output side while keeping the voltage steady on the load side. Although the load percentage will drop by about 50 %, the DC link voltage initially rises. The voltage control element detects this deviation and reduces the power transfer from the source. Meanwhile, the supercapacitor absorbs the variation and keeps operations stable. The hybrid energy mechanism improves damping and reduces overshoot, which can be difficult with advanced control methods.

Similarly, during a disturbance at the source or a temporary failure of any input source, the energy management system redistributes power based on demand. The PI current limit loop stops excessive current from rising. The converter stays operational even during a sudden voltage drop. Even with large signal transients, such as 50 % load reduction or source failure, the characteristics of the hybrid architecture help manage disturbances and enhance stability.

This proposed system enables multiple energy sources to connect simultaneously to a single DC bus for traction inverters. These systems enable modular electric vehicle architectures, allowing future improvements without requiring a complete powertrain overhaul. Isolated converters enhance energy management and reduce the number of components, thus improving power density and creating more space for additional EV subsystems. The proposed design reduces battery stress from excessive continuous use, enhances charge-discharge cycles, and maintains overall health by providing a secondary energy source. Moreover, the proposed system functions as a mobile energy hub for intelligent grids and facilitates hybridization that extends beyond traditional batteries, thus enabling the smooth integration of hybrid energy. Therefore, the sustained alignment system will incorporate advanced frameworks for green energy systems.

CONFLICTS OF INTEREST

The authors declare that they have no conflicts of interest.

REFERENCES

[1] S. B. Sudarshan and G. Arunkumar, “Isolated DC-DC power converters for simultaneous charging of electric vehicle batteries: Research review, design, high-frequency transformer testing, power quality concerns, and future”, *Sustainability*, vol. 15, no. 3, p. 2813, 2023. DOI: 10.3390/su15032813.

[2] B. Le-Huy Nguyen, H. Cha, T. Vu, and T.-T. Nguyen, “Integrated multiport bidirectional DC-DC converter for HEV/FCV applications”, in *Proc of the 47th Annual Conference of the IEEE Industrial Electronics Society (IECON)*, 2021, pp. 1–6. DOI: 10.1109/IECON48115.2021.9589188.

[3] Y. Tong, I. Salhi, Q. Wang, G. Lu, and S. Wu, “Bidirectional DC-DC converter topologies for hybrid energy storage systems in electric vehicles: A comprehensive review”, *Energies*, vol. 18, no. 9, p. 2312, 2025. DOI: 10.3390/en18092312.

[4] K. Itoh, M. Ishigaki, N. Yanagizawa, S. Tomura, and T. Umeno, “Analysis and design of a multiport converter using a magnetic coupling inductor technique”, *IEEE Transactions on Industry Applications*, vol. 51, no. 2, pp. 1713–1721, 2015. DOI: 10.1109/TIA.2014.2354401.

[5] E. Martinez-Vera and P. Banuelos-Sanchez, “Review of bidirectional DC-DC converters and trends in control techniques for applications in electric vehicles”, *IEEE Latin America Transactions*, vol. 22, no. 2, pp. 144–155, 2024. DOI: 10.1109/tla.2024.10412031.

[6] T. B. Nkwanyana, M. W. Siti, Z. Wang, I. Toudjeu, N. T. Mbungu, and W. Mulumba, “An assessment of hybrid-energy storage systems in the renewable environments”, *Journal of Energy Storage*, vol. 72, part C, art. 108307, 2023. DOI: 10.1016/j.est.2023.108307.

[7] C.-C. Hua and J.-B. Lai, “A bidirectional isolated DC-to-DC converter with hybrid control of pulse width modulation and pulse frequency modulation”, *Processes*, vol. 12, no. 12, p. 2866, 2024. DOI: 10.3390/pr12122866.

[8] D. Xu, Q. Liu, W. Yan, and W. Yang, “Adaptive terminal sliding mode control for hybrid energy storage systems of fuel cell, battery and supercapacitor”, *IEEE Access*, vol. 7, pp. 29295–29303, 2019. DOI: 10.1109/ACCESS.2019.2897015.

[9] J. Huang *et al.*, “Rational design of electrode materials for advanced supercapacitors: From lab research to commercialization, advanced functional materials”, *Advanced Functional Materials*, vol. 33, no. 14, art. 2213095, 2023. DOI: 10.1002/adfm.202213095.

[10] X. Wang, Y. Luo, B. Qin, and L. Guo, “Power allocation strategy for urban rail HESS based on deep reinforcement learning sequential decision optimization”, *IEEE Transactions on Transportation Electrification*, vol. 9, no. 2, pp. 2693–2710, 2023. DOI: 10.1109/TTE.2022.3227900.

[11] Y. bin Yu, X. Liu, H. Min, H. Sun, and L. Xu, “A novel fuzzy-logic based control strategy for a semi-active battery/super-capacitor hybrid energy storage system in vehicular applications”, *Journal of Intelligent & Fuzzy Systems*, vol. 29, no. 6, pp. 2575–2584, 2015. DOI: 10.3233/IFS-151960.

[12] S. Farajdadian, A. Hajizadeh, and M. Soltani, “Recent developments of multiport DC/DC converter topologies, control strategies, and applications: A comparative review and analysis”, *Energy Reports*, vol. 11, pp. 1019–1052, 2024. DOI: 10.1016/j.egyr.2023.12.054.

[13] N. Guennouni, N. Machkour, and A. Chebak, “Single- and three-phase dual-active-bridge DC–DC converter comparison for battery electric vehicle powertrain application”, *Energies*, vol. 17, no. 21, p. 5509, 2024. DOI: 10.3390/en17215509.

[14] A. Wangsupphaphol, S. Phichaisawat, N. R. Nik Idris, A. Jusoh, N. D. Muhamad, and R. Lengkayan, “A systematic review of energy management systems for battery/supercapacitor electric vehicle applications”, *Sustainability*, vol. 15, no. 14, p. 11200, 2023. DOI: 10.3390/su151411200.

[15] S. Negri, G. Ubezio, and R. S. Faranda, “Fault-tolerant multiport converter for hybrid distribution systems: Configuration, control principles and fault analysis”, *Applied Science*, vol. 14, no. 10, p. 4024, 2024. DOI: 10.3390/app14104024.

[16] M. M. Savrun and A. Atay, “Multiport bidirectional DC–DC converter for PV powered electric vehicle equipped with battery and supercapacitor”, *IET Power Electronics*, vol. 13, no. 17, pp. 3931–3939, 2020. DOI: 10.1049/iet-pel.2020.0759.

[17] M. Prabhakar, F. L. Tofoli, M. A. Elgendy, and H. Wang, “Modelling, design and control of power electronic converters for smart grids and electric vehicle applications”, *IET Power Electronics*, vol. 17, no. 9, pp. 983–985, 2024. DOI: 10.1049/pel2.12715.

[18] H. Akagi, S.-i. Kinouchi, and Y. Miyazaki, “Bidirectional isolated dual-active bridge (DAB) DC–DC converters using 1.2-kV 400-A SiC-MOSFET dual modules”, *CPSS Transactions on Power Electronics Application*, vol. 1, no. 1, pp. 33–40, 2016. DOI: 10.24295/CPSSTPEA.2016.00004.

[19] J. Lu, Y. Wang, X. Li, and C. Du, “High-conversion-ratio isolated bidirectional DC–DC converter for distributed energy storage systems”, *IEEE Transactions on Power Electronics*, vol. 34, no. 8, pp. 7256–7277, 2019. DOI: 10.1109/TPEL.2018.2881085.

[20] E. L. Carvalho, E. G. Carati, J. P. da Costa, C. M. de Oliveira Stein, and R. Cardoso, "Analysis, design and implementation of an isolated full-bridge converter for battery charging", in *Proc. of 2017 Brazilian Power Electronics Conference (COBEP)*, 2017, pp. 1–6. DOI: 10.1109/COBEP.2017.8257344.

[21] I. A. Sayed and Y. Mahmoud, "Energy management of battery–supercapacitor hybrid storage in electric vehicles with solar integration: A review", *IEEE Access*, vol. 13, pp. 200555–200583, 2025. DOI: 10.1109/ACCESS.2025.3636410.

[22] M. B. Camara, H. Gualous, F. Gustin, and A. Berthon, "Design and new control of DC/DC converters to share energy between supercapacitors and batteries in hybrid vehicles", *IEEE Transactions on Vehicular Technology*, vol. 57, no. 5, pp. 2721–2735, 2008. DOI: 10.1109/TVT.2008.915491.

[23] J. Hong, J. Yin, Y. Liu, J. Peng, and H. Jiang, "Energy management and control strategy of photovoltaic/battery hybrid distributed power generation systems with an integrated three-port power converter", *IEEE Access*, vol. 7, pp. 82838–82847, 2019. DOI: 10.1109/ACCESS.2019.2923458.

[24] J. Zeng, W. Qiao, and L. Qu, "An isolated three-port bidirectional DC-DC converter for photovoltaic systems with energy storage", in *Proc. of 2013 IEEE Industry Applications Society Annual Meeting*, 2013, pp. 1–8. DOI: 10.1109/IAS.2013.6682520.

[25] S. Pourjafar, H. Shayeghi, F. Sedaghati, S. Seyedshenava, and F. Blaabjerg, "A bidirectional multiport DC-DC converter applied for energy storage system with hybrid energy sources", *International Journal of Circuit Theory and Applications*, vol. 49, no. 8, pp. 2453–2478, 2021. DOI: 10.1002/cta.2988.

[26] F. Akar, Y. Tavlasoglu, and B. Vural, "An energy management strategy for a concept battery/ultracapacitor electric vehicle with improved battery life", *IEEE Transactions on Transportation Electrification*, vol. 3, no. 1, pp. 191–200, 2017. DOI: 10.1109/TTE.2016.2638640.

[27] S. Khosrogorji, M. Ahmadian, H. Torkaman, and S. Soori, "Multi-input DC/DC converters in connection with distributed generation units – A review", *Renewable and Sustainable Energy Reviews*, vol. 66, pp. 360–379, 2016. DOI: 10.1016/j.rser.2016.07.023.

[28] N. A. Ahmed and J. Y. Madouh, "High-frequency full-bridge isolated DC–DC converter for fuel cell power generation systems", *Electrical Engineering*, vol. 100, pp. 239–251, 2018. DOI: 10.1007/s00202-016-0499-6.

[29] S. Hu, Z. Liang, and X. He, "Ultracapacitor-battery hybrid energy storage system based on the asymmetric bidirectional Z-source topology for EV", *IEEE Transactions on Power Electronics*, vol. 31, no. 11, pp. 7489–7498, 2016. DOI: 10.1109/TPEL.2015.2493528.



This article is an open access article distributed under the terms and conditions of the Creative Commons Attribution 4.0 (CC BY 4.0) license (http://creativecommons.org/licenses/by/4.0/).